Received: 23 May 2020 | Revised: 4 December 2020 | Accepted: 7 December 2020

DOI: 10.1002/esp.5049

RESEARCH ARTICLE

ESPL WILEY

The spatial distribution of sedimentary compounds and their environmental implications in surface sediments of Lake Khar Nuur (Mongolian Altai)

P. Strobel | J. Struck | R. Zech | M. Bliedtner

Physical Geography, Institute of Geography, Friedrich Schiller University Jena, Jena, Germany

Correspondence
Paul Strobel, Physical Geography, Institute of Geography, Friedrich Schiller University Jena, Loebdergraben 32, 07743. Jena, Germany.
Email: paul.strobel@uni-jena.de

Abstract

Lake sediments are valuable natural archives to reconstruct paleoclimate and paleoenvironmental changes which consist of inorganic and organic sediment compounds of allochthonous origin from the catchment and of autochthonous production in the lake. However, for robust paleo-reconstructions it is important to develop a better understanding about sedimentation processes, the origin of inorganic and organic sediment compounds and their distribution within the lake. In this context, modern process studies provide important insights, although environmental and anthropological changes can affect the spatial distribution of sediment compounds through time. Therefore, in this study the spatial distribution of grain size and geochemical proxies in 52 surface sediment samples from Lake Khar Nuur, a small high-altitude lake in the Mongolian Altai with a small and anthropogenically used hydrological catchment, is investigated. The results show a distinct sediment focussing in the two deep basins of the lake, which therefore act as accumulation zones. In those accumulation zones, total organic carbon (TOC), total nitrogen (N) and their isotopic composition ($\delta^{13}C_{TOC}$, $\delta^{15}N$) as well as *n*-alkanes indicate that organic sediment compounds are a mixture of both allochthonous and autochthonous origin. While the recent catchment vegetation consists of grasses/herbs and the shrub *Betula nana* (L.) with distinct differences in their *n*-alkane homologue patterns, those differences are not reflected in the sediment surface samples which rather indicates that grass-derived *n*-alkanes become preferentially incorporated in the lake. Extensive anthropogenic activity such as grazing and housing in the southern part of the catchment causes soil erosion which is well reflected by high TOC, N and sulphur (S) contents and ^{15}N depleted $\delta^{15}N$ values at the central southern shore, i.e. increased allochthonous sediment input by anthropogenically-induced soil erosion. Overall, the surface sediments of Lake Khar Nuur origin from allochthonous and autochthonous sources and are focussed in the accumulation zones of the lake, while their distribution is both environmentally and anthropogenically driven.

KEYWORDS
geochemistry, grain size, lake sediments, *n*-alkanes, sediment focussing, stable isotopes

1 | INTRODUCTION

Lake sediments are valuable natural archives providing long records of past limnological, hydrological, and anthropological change. However, robust reconstructions require an understanding of how sediments and the recent climate/environmental signals are incorporated into the sediment archive and how the sediment archive is distributed within the lake basin. Studies investigating the composition and spatial distribution of lake surface sediments have a long history in the field of limnology. Over the last decades, the spatial distribution of sedimentological, inorganic, organic and biogeochemical proxies (Anderson et al., 2008; Dearing, 1997; Ju et al., 2010; Kastner et al., 2010; Shuman, 2003; Thomas et al., 1972; Vogel et al., 2010; Wang et al., 2015; Yu et al., 2015; Yu et al., 2018), as well as heavy metals (Guo et al., 2018; Moore, 1980; Onyari & Wandiga, 1989), pollen (DeBusk, 1997; Li, 2018, 2019; Zhao et al., 2006), diatoms and ostracods (Anderson, 1990; Martens & Tudorancea, 1991; Shah et al., 2017; Yu et al., 2019; Zalat & Vildary, 2005) was analysed in lake surface sediment samples by several studies. While most of these studies show that sediments and sedimentary compounds accumulate in the deep basins within lakes (i.e. sediment focussing), they mainly focussed on large hydrological settings with large lake surfaces. Therefore the spatial resolution of the analyses and the related process understanding are limited due to the low sample size compared to the lakes surface. Thus, there is a lack of studies investigating lake surface sediments in high spatial resolution to gain a better understanding about modern sedimentation processes, the origin of different sedimentary compounds and their distribution within the lake.

Sedimentary processes in hydrological systems can best be understood by the grain size and elemental [e.g. aluminium (Al), iron (Fe)] distribution which is directly related to transport mechanisms and transport energies and indicate allochthonous input into the lake (Håkanson & Jansson, 1983; Mclaren & Bowles, 1985; Wen et al., 2008; Wündsch et al., 2018). Both proxies can be used to trace sediment focussing in deeper parts of the lake below the mud deposition boundary (Anderson et al., 2008; Lehman, 1975; Wang et al., 2015). The origin of organic sedimentary compounds in lake sediments (allochthonous vs. autochthonous) can be disentangled by total organic carbon (TOC) and total nitrogen (N) contents, as well as their stable carbon and nitrogen isotopes (Meyers, 1994; Meyers, 2003). Since TOC can represent a heterogeneous organic matter pool in lake sediments that comprises organic carbon of different origins and preservation states, *n*-alkanes can be complementary for source detection. They are a more homogenous part of the organic matter pool, and depending on their chain-length distribution, they are of autochthonous (aquatic) or allochthonous (terrestrial) origin. While *n*-alkanes produced by aquatic (submerged) macrophytes have a dominance of the shorter chains nC_{21} and nC_{23} (Ficken et al., 2000; Sachse et al., 2004), *n*-alkanes produced in the leaf waxes of higher terrestrial plants have a dominance on the longer chains from nC_{27} to nC_{35} (Eglinton & Eglinton, 2008; Shepherd & Wynne Griffiths, 2006). Besides being source-specific, the homologue patterns of leaf wax *n*-alkanes can be used to differentiate between vegetation types. Although homologue patterns can have limited differentiation power on a global scale (Bush & McInerney, 2013), they can differentiate well between grasses and herbs (i.e. nC_{31} and nC_{33}) and woody shrubs and deciduous trees (i.e. nC_{27} and nC_{29}) in many regions of the world including semi-arid Mongolia (Bliedtner et al., 2018; Liu et al., 2018; Schäfer et al., 2016; Struck et al., 2020). Up to now, studies analysing the spatial distribution of *n*-alkanes and their origin in surface sediment samples are very limited (Wang et al., 2015), and studies that combine both sedimentological and inorganic as well as organic and biogeochemical proxies in small lakes with small catchments and a clearly defined catchment-geomorphology are still scarce. However, such lakes and their respective catchments have the great advantage of a high sediment connectivity, that is rapid sediment transport from the catchment into the lake, while sediment re-working in the lake is limited (Oldfield, 1977).

Therefore, the aim of this study is to investigate the spatial distribution of sedimentological and geochemical proxies of surface sediments in Lake Khar Nuur, a small high-altitude lake with a small drainage basin in the Mongolian Altai. We aim to develop a better understanding about recent sedimentation processes, the origin of different sedimentary compounds and how those compounds are distributed within the lake. Although environmental changes can affect the spatial distribution of sediment compounds through time, we further aim to improve proxy-understanding and paleoenvironmental interpretations using modern analogues in lake sediments. More specifically, we address the following objectives:

- We will investigate the origin and focussing of allochthonous and autochthonous inorganic and organic sediment compounds in the lake by grain size distribution, elemental composition (Al, Fe), TOC and N and their stable isotopes ($\delta^{13}C_{TOC}$, $\delta^{15}N$) as well as *n*-alkanes.
- We will investigate distinct differences in the vegetation types of the catchment by leaf wax *n*-alkane homologue patterns and if those vegetation types can also be detected in the lakes surface sediments.
- We will identify traces of anthropogenic activity and soil erosion in the catchment in the lakes surface sediments by elemental sulphur (S) as well as TOC and N contents and their stable isotopes.

2 | STUDY SITE

Lake Khar Nuur is a small para-glacial lake located at 2,486 m above sea level (a.s.l.) in the Mongolian Altai (48°37′N, 88°56′E) and has a

small drainage basin (44.8 km^2) that covers altitudes from 2,486 to 3,156 m a.s.l. (Figure 1a, b). Glacial advances from the south-western slopes of the Tsengel Khairkhan Mountains left prominent moraine lobes during the last glaciation which blocked the valley and formed the endorheic Khar Nuur basin (Figure 1b) (Walther et al., 2017). The bedrock of most parts of the catchment is composed of friable black clay shales, whereas only the morainal deposits in the western parts of the catchment consist of granite. Steep slopes (>16°) occur in the northern, western and south-eastern parts of the catchment, but flatter areas are noticeable in the central southern part (Figures 1c, 2a). On the steep slopes of the catchment, very shallow Leptosols occur, whereas Mollisols with humus rich topsoils (~50 cm) and underlying permafrost developed in the flatter areas of the central southern part of the catchment. At those flatter areas, several gullies exist (Figures 1b, 2c) and favour increased runoff and sediment transport into the lake during snowmelt and precipitation events. The other parts of the catchment only produce little episodic runoff and no perennial inflow into the lake exists (Figure 1b, c). Today, most parts of the catchment are anthropogenically used during the summer month, although the central southern part is preferential used by grazing and nomadic housing (Figure 1d). Additionally, a road was constructed around the southern part of the lake (Figure 2b).

At the nearest climate station Tolbo Sum (CDC-ID 44217), which is located ~90 km southeast of Lake Khar Nuur at an altitude of ~2,100 m a.s.l., mean annual precipitation sum was 145 ± 35 mm (2009–2017) and mean annual temperature was −2.4 ± 0.7°C (2009–2019) (DWD Climate Data Center, 2020). The number of ice days (maximum air temperature below 0°C) and freeze days (minimum

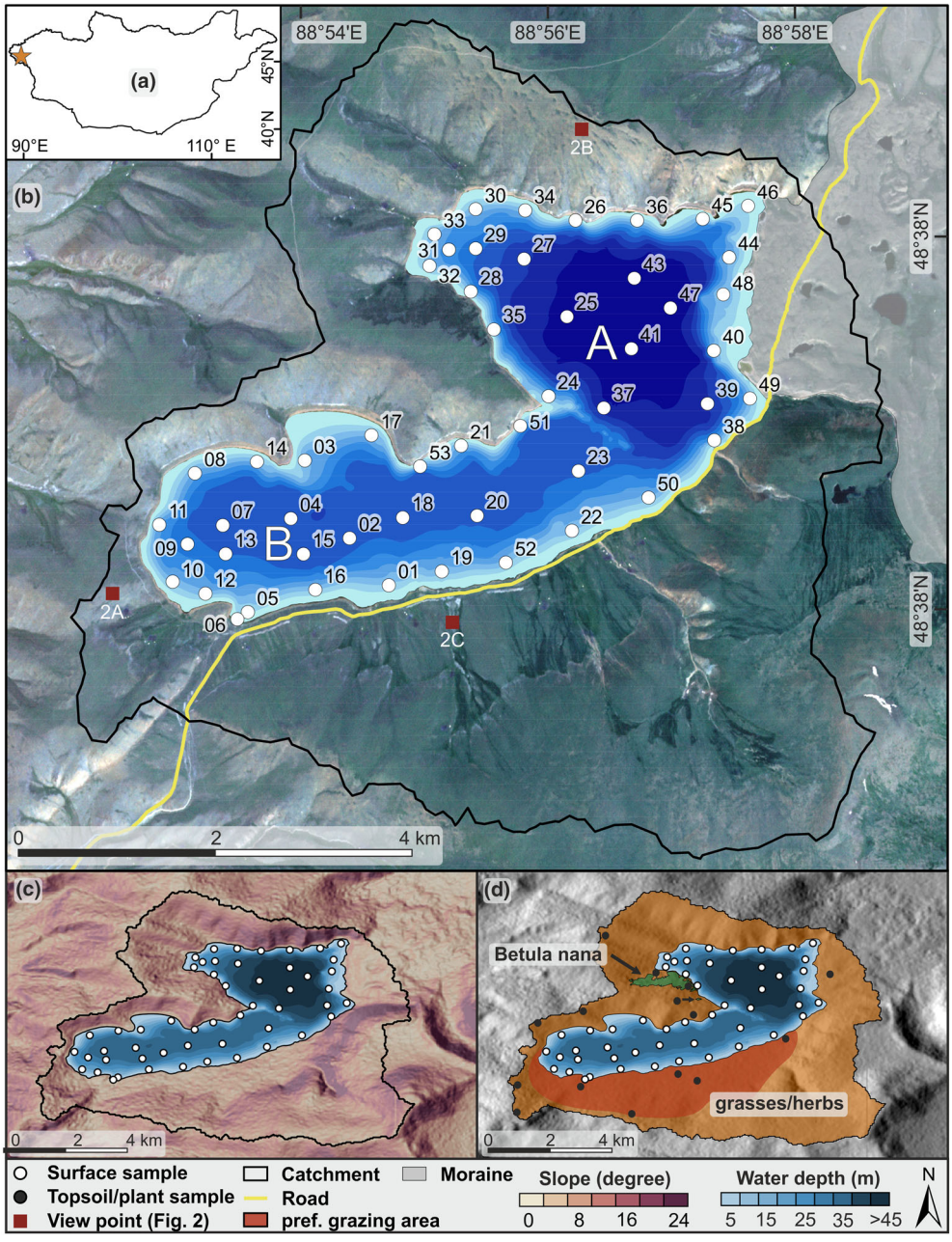

FIGURE 1 (a) Location of the study site in western Mongolia. (b) Satellite image of the study site with the hydrological catchment of Lake Khar Nuur, the lake bathymetry with the two basins A and B, the surface sediment sample locations with sample identification (ID) and the viewpoints of the images in Figure 2. The grey shaded area shows the morainal deposits. (c) Topographic map of Lake Khar Nuur. (d) Vegetation distribution and preferential grazing area in the catchment of Lake Khar Nuur. White and black dots indicate lake surface sediment and topsoil/plant samples in (c) and (d) [data source – bathymetry: own data; satellite image: Planet Team (2017), SRTM 1 arc second (~30 m × 30 m)]

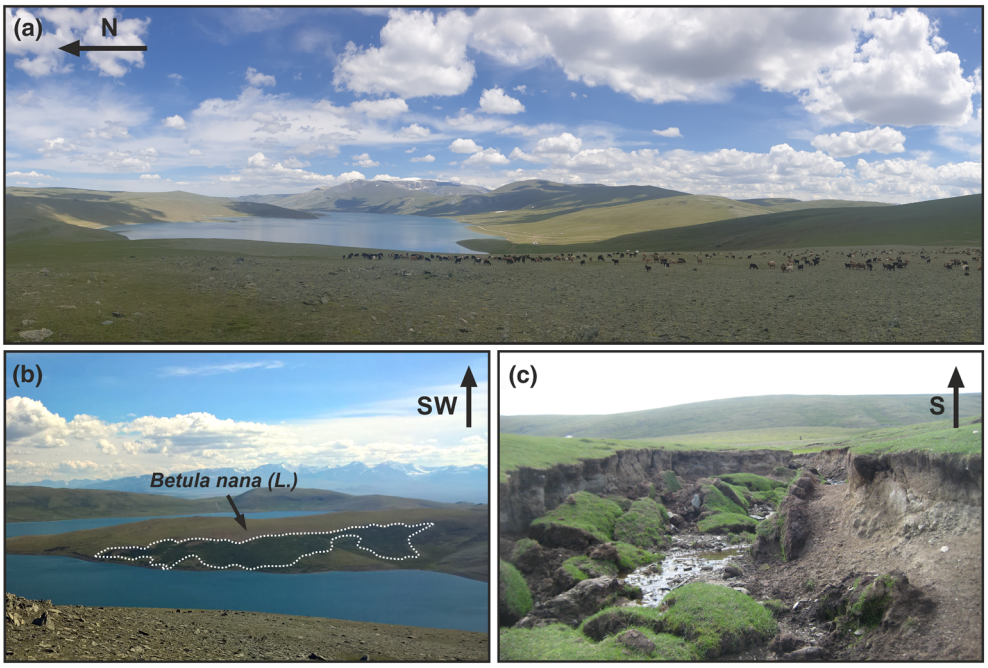

FIGURE 2 Photographs from Lake Khar Nuur and its catchment. (a) Overview of the lake showing the steep slopes in the northern part and the flatter areas in the central southern part of the catchment, and grazing in the front of the picture. (b) Parts of the catchment that are grown with *Betula nana* (L.). (c) Gully erosion in the central southern part of the catchment (photograph by W. Zech)

air temperature < 0°C) were 140 and 247, respectively (DWD Climate Data Center, 2020). Since Lake Khar Nuur is located ~385 m higher than Tolbo Sum, even lower mean annual temperatures as well as more ice and freeze days can be expected. Consequently, the surface of Lake Khar Nuur is ice covered for eight to nine months per year (2016–2019; Planet Team, 2017). The harsh environmental conditions lead to the dominance of alpine grasses and herbs in the Khar Nuur catchment. Exceptional are small patches of 50 to 80 cm high *Betula nana* (L.) shrubs that covers a small area (~0.42 km^2) with favourable edaphic conditions on a north-eastern slope (Figures 1d, 2b).

3 | MATERIAL AND METHODS

3.1 | Bathymetry

A bathymetric map of the lake floor was created using a Lowrance HPS 5 Fishfinder working with a frequency of 100 kHz. A ~240,000 depth-measurements were conducted and the respective drive-lines are shown in Figure 3(a). The map was created using the software Sonar Viewer 2.1.2 and Esri ArcGIS 10.5 applying the 'spline with barriers' interpolation tool.

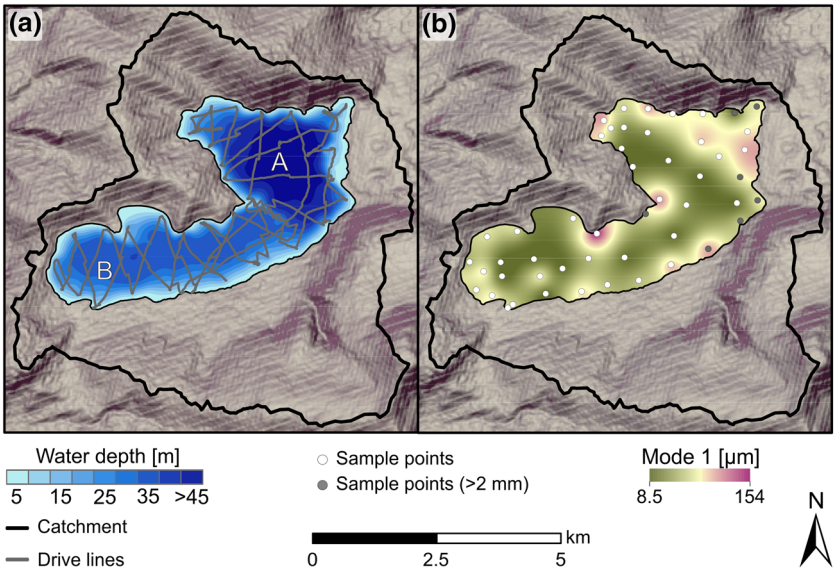

FIGURE 3 (a) Echo-sounder drive lines (grey lines) for the creation of the bathymetric map of Lake Khar Nuur with the two basins A and B. (b) Mode 1 grain size distribution of the sediment samples from Lake Khar Nuur. White circles show sample points and grey circles indicate the presence of sediments > 2 mm within the surface sediment samples in the lake. Black line indicates the catchment of Lake Khar Nuur [data source – SRTM 1 arc second (30 m × 30 m)]

3.2 | Sampling and laboratory analyses

For this study, the sediment surface (0–1 cm) of the lake floor was sampled at 52 locations (for sample locations see Figure 1b) using a Van Veen Grab sampler (Lie & Pamatmat, 1965). All samples are from a water depth > 2 m (Figure 1a). Except for grain size analyses, samples were freeze-dried (−50°C; > 72 h), ground and sieved to < 40 μm.

3.3 | Grain size analyses

For grain size analyses, sample aliquots were treated with hydrogen peroxide (H_2O_2, 15%, 30%) to remove organic matter and subsequently treated with hydrochloric acid (HCl, 15%) to remove carbonates. As a dispersant, 5 ml sodium-pyrophosphate ($Na_4P_2O_7{\cdot}10\ H_2O$) were added to each sample and shaken for > 2 h. Before the measurement, the fraction > 2 mm was removed from the samples by sieving due to technical reason. It has to be noted that the > 2 mm fraction was only present in the samples 38, 40, 45, 46, 48, 50 and 51 (grey sample points in Figure 3b), which, however, was not further quantified. The < 2 mm grain-size distribution was determined with a laser diffraction particle size analyzer (LS 13320, Beckman Coulter, Brea, California, USA). Samples were measured with the aqueous liquid module in several 60 s cycles until a reproducible signal was obtained. The 'Fraunhofer' optical model of light scattering was used for computing grain size distribution. In the following we will use Mode 1 which is the most frequently occurring particle size and was calculated with a modified version of the Software Gradistat 4.2 (Blott & Pye, 2001).

3.4 | Elemental analyses

Al, Fe and S concentrations were measured with an ICP-OES 725-ES (VARIAN, Palo Alto, California, USA). Samples (0.2 g) were dissolved using a microwave-assisted modified aqua regia digestion of 2 ml HCl (32%), 4 ml nitric acid (HNO_3, 65%), 1 ml H_2O_2 (30%) and 6 ml deionized water. For error estimation, two samples (KN09, KN41) were measured in triplicates (relative error: Al, 1.6%; Fe, 1.6%; S, 11%). Additionally, the reference material LGC6 187 (river sediment, $n = 8$) was measured to calculate the relative analytical error, which was < 2.0%.

3.5 | Carbon and nitrogen analyses and bulk isotopic analyses

Carbon and nitrogen contents and their stable isotopes were analysed with an Elementar Analyser (vario EL cube) coupled to an isotope ratio mass spectrometer (Isoprime precision). ~30 mg of untreated sediment per sample was weighted into tin boats (Elementar, 6 × 6 × 12) and measured for total carbon (TC), total nitrogen (N) and the nitrogen isotopic composition ($\delta^{15}N$). Prior to the analyses of TOC and the carbon isotopic composition ($\delta^{13}C$), carbonates were removed from the samples with 1 N HCl at 60°C for 8 h. Samples were subsequently washed with ultrapure water to pH neutrality and ~30 mg were weighted into tin boats. The analytical precision of the $\delta^{15}N$ and $\delta^{13}C$ analyses was checked against certified standards (L-Prolin, EDTA and USGS65), and gave an analytical error < 0.25‰ and < 0.05‰, respectively. The $\delta^{15}N$ and $\delta^{13}C$ are given in their delta notation against Air and the Vienna Pee Dee Belemnite (VPDB).

Total inorganic carbon (TIC) was calculated by subtracting TOC from TC. The molar ratio of TOC and N was calculated based on their respective molecular weights (Equation (1)). Relative errors were calculated based on triplicate measurements (TC: < 0.1%, N: < 0.9%, TOC: < 0.8%).

$$\mathrm{TOC/N\,[molar]} = \mathrm{TOC\,[\%]} \cdot 12.0107\left[\mathrm{g\cdot mol^{-1}}\right] / \mathrm{N\,[\%]} \cdot 14.0067\left[\mathrm{g\cdot mol^{-1}}\right] \quad (1)$$

3.6 | Leaf wax analyses

Total lipids of 49 surface sediment samples, 13 topsoil samples (5–28 g, depending on bulk density and TOC content) and seven plant samples (0.8–1.1 g) were extracted with 40 ml dichloromethane (DCM) and methanol (MeOH) (9:1, *v/v*). According to Bliedtner et al. (2018), each sample was ultrasonically extracted over three 15 min cycles. The total lipid extract was separated by solid phase extraction using aminopropyl silica gel (Supelco, 45 μm, Bellefonte, Pennsylvania, USA) as a stationary phase. The *n*-alkanes were eluted with 4 ml hexane and further purified over coupled silver nitrate ($AgNO_3$)–zeolite (Geokleen, Bebington, Merseyside, UK) pipette columns. The *n*-alkanes trapped in the zeolite were subsequently dissolved in hydrofluoric acid and recovered by liquid–liquid extraction using hexane.

An Agilent 7890B gas chromatograph equipped with an Agilent HP5MS column (30 m, 320 μm, 0.25 μm film thickness) and a flame ionization detector (FID) was used for identification and quantification of the *n*-alkanes, relative to external *n*-alkane standards (*n*-alkane mix nC_{21}–nC_{40}, Supelco, Bellefonte, Pennsylvania, USA). Precision of compound quantification was about 1.2% based on multiple measurements of the external standard ($n = 10$).

n-Alkane concentrations ($\sum n$-alkanes) are given in μg g^{-1} dry weight and were calculated as the sum of nC_{21} to nC_{35}. The odd-over-even predominance (OEP) was calculated according to Hoefs et al. (2002) (Equation 2) and serves as a proxy for degradation with values below five indicating enhanced *n*-alkane degradation (Buggle et al., 2010; Zech et al., 2010).

$$\mathrm{OEP} = \left(\frac{nC_{27} + nC_{29} + nC_{31} + nC_{33}}{nC_{26} + nC_{28} + nC_{30} + nC_{32}}\right) \quad (2)$$

We used a normalized *n*-alkane ratio that we modified according to the differences between the two prominent vegetation forms in the Khar Nuur catchment and that we calculated to detect possible contributions from those vegetation forms in the surface sediments. Differences in the respective vegetation forms are because nC_{31} is the most abundant *n*-alkane of grasses/herbs and nC_{27} of the shrub *Betula nana* (L.) (see Results 4.3; Equation 3).

$$n-\text{alkane ratio} = \frac{nC_{31}}{nC_{27} + nC_{31}} \quad (3)$$

To further obtain information about *n*-alkane contributions from aquatic and terrestrial plants in our surface sediment samples, we quantify the relative contribution of *n*-alkanes derived from submerged and floating macrophytes relative to *n*-alkanes derived from leaf waxes of terrestrial plants (P_{aq}' ratio; Equation 4; modified after Ficken et al., 2000). Aquatic plants (of submerged macrophyte origin) are dominated by short-chain *n*-alkanes (typically nC_{21} and nC_{23}; e.g. Sachse et al., 2004). Grasses/herbs and shrubs show a nC_{31} and nC_{29} predominance in Mongolia (Struck et al., 2020).

$$Paq' = \frac{nC_{21} + \cdot nC_{23}}{nC_{21} + nC_{23} + nC_{29} + nC_{31}} \quad (4)$$

3.7 | Data analyses

The hydrological Khar Nuur catchment and its geomorphological attributes were derived from a digital elevation model (SRTM) with a spatial resolution of ~30m × 30 m. Based on the sedimentological and geochemical results of the surface sediment samples, spatial distribution maps were generated using the 'spline with barriers' tool in Esri ArcGIS 10.5. Pearson's *r*-values were calculated to detect correlations of the analysed proxies and a student's *t*-test was performed to determine significant differences (α = 0.05). All statistical analyses were performed using the statistical software OriginPro 2017.

4 | RESULTS

4.1 | Bathymetry and grain size distribution

The bathymetric map of Lake Khar Nuur shows two basins within the lake. Following the morphology of the catchment, the first basin in the northeast of the lake (basin A; Figures 1b, 3a) shows sub-aquatic steep slopes and a large plain in the centre with the deepest part 49.4 m below lake level (Figures 1b, 3a). In the southwest of the lake, a second basin is present (basin B, Figures 1b, 3a) and the sub-aquatic slopes also follow the catchment's morphology with steep slopes on the northern shore and distinctly flatter slopes on the southern shore. Both basins are separated by a sub-aquatic ridge that follows the distinct ridge in the north-western part of the catchment (Figures 1b, c, 3a).

The Mode 1 of the grain size distribution shows highest values (coarse silt to fine sand) at the shore of basin A, but also below the steep slopes in basin B (Figure 3b). The finer grain size fractions (smaller than coarse silt) as indicated by low Mode 1 values accumulate in the centre of both basins (Figure 3b). This is well reflected by a significant anti-correlation of Mode 1 and water depth (r = –0.45; α < 0.05; Table 1), indicating fine grained sediments at greater water depth and vice versa. We have to note that particles > 2 mm were detected within samples 38, 40, 45, 46, 48, 50 and 51 (grey sample points in Figure 3b), but not further quantified. So, Mode 1 values are only representative for the < 2 mm fraction.

4.2 | Elemental distribution, carbon and nitrogen contents and bulk isotopic composition

The elemental distribution in Lake Khar Nuur surface sediments shows highest concentrations of Al (42,900 ± 3,900–58,700 ± 4,500 ppm) and Fe (32,500 ± 1,400–51,000 ± 2,200 ppm) in the central and deepest parts of basins A and B, whereas the nearshore samples show lowest concentrations (Al: < 40,900 ± 3,300 ppm; Fe: < 27,000 ± 1,200 ppm) (Figure 4a, b). Sulphur (S) also shows high concentrations in the deepest parts in both basins, but highest concentrations occur at the central southern shore (4,900 ± 1,500 ppm). All other nearshore samples and samples at the sub-aquatic ridge show low concentrations (< 1,000 ± 100 ppm) (Figure 4c).

A similar spatial distribution to S is shown by TOC and N with highest concentrations in the deepest parts in both basins A and B (TOC: 3.8–4.7%, N: 0.6–0.7%) and high concentration at the central southern shore. Low concentrations are shown by the nearshore samples and samples at the sub-aquatic ridge (TOC: < 2.01 ± 0.01%; N: < 0.44 ± 0.01%) (Figure 4d, e). The spatial distribution of TIC shows the highest concentrations in basins A and B and at the central southern shore (2.21 ± 0.04 to 3.11 ± 0.06%), whereas the remaining nearshore samples and samples at the sub-aquatic ridge show low concentrations (< 2.06 ± 0.04%) (Figure 4f).

The isotopic composition of TOC ($\delta^{13}C_{TOC}$) ranges from –29.0‰ to –19.5‰ (Figure 4g). For most parts of the lake, the samples show ^{13}C depleted $\delta^{13}C_{TOC}$ values, whereas $\delta^{13}C_{TOC}$ values are enriched in ^{13}C at the northern shoreline and for two samples at the southern shoreline (KN19 and KN52, Figure 4g). The nitrogen isotopic composition ($\delta^{15}N$) ranges between 1.7‰ and 4.8‰ (Figure 4h). While most parts of the lake are enriched in ^{15}N, samples are remarkably depleted in ^{15}N at the central southern shore (Figure 4h). The molar TOC/N ratio shows higher values in both basins A and B compared to the nearshore samples (Figure 4i). However, the molar TOC/N ratio ranges between 1.22 and 6.60 and reflects only a very small range.

TABLE 1 Correlation matrix (Person's *r*) of the investigated proxies

	WD	Mode 1	Al	Fe	S	TOC	$\delta^{13}C$	N	$\delta^{15}N$	TIC	TOC/N	C_{21}	C_{31}	*n*-Alkane-concentration	OEP	*n*-Alkane-ratio
Mode 1	**−0.45**															
Al	**0.87**	**−0.49**														
Fe	**0.81**	**−0.55**	**0.86**													
S	0.23	−0.17	**0.28**	0.25												
TOC	**0.75**	**−0.39**	**0.80**	**0.67**	**0.66**											
$\delta^{13}C$	**−0.72**	**0.40**	**−0.68**	**−0.62**	−0.19	**−0.64**										
N	**0.71**	**−0.39**	**0.75**	**0.67**	**0.76**	**0.96**	**−0.60**									
$\delta^{15}N$	**0.35**	−0.17	0.24	**0.36**	**−0.47**	−0.08	**−0.41**	−0.14								
TIC	**0.56**	**−0.28**	**0.61**	**0.52**	**0.63**	**0.69**	**−0.40**	**0.79**	**−0.33**							
TOC/N	**0.59**	**−0.35**	**0.64**	**0.53**	**0.39**	**0.83**	**−0.64**	**0.70**	0.08	**0.33**						
C_{21}	**0.75**	−0.28	**0.78**	**0.56**	**0.40**	**0.85**	**−0.66**	**0.78**	−0.01	**0.66**	**0.67**					
C_{31}	**0.75**	**−0.35**	**0.81**	**0.64**	**0.44**	**0.88**	**−0.71**	**0.83**	0.03	**0.67**	**0.73**	**0.94**				
n-Alkane-concentration	**0.76**	**−0.33**	**0.81**	**0.62**	**0.47**	**0.90**	**−0.70**	**0.85**	−0.01	**0.69**	**0.72**	**0.97**	**0.99**			
OEP	**−0.62**	**0.37**	**−0.66**	**−0.58**	−0.22	**−0.58**	**0.35**	**−0.59**	−0.08	**−0.62**	**−0.37**	**−0.62**	**−0.55**	**−0.60**		
Alkane-ratio	−0.23	0.12	−0.26	−0.20	**−0.74**	**−0.63**	0.27	**−0.70**	**0.44**	**−0.56**	**−0.45**	**−0.43**	**−0.39**	**−0.45**	**0.47**	
P_{aq}'	**0.67**	**−0.31**	**0.70**	**0.54**	**0.53**	**0.84**	**−0.58**	**0.82**	−0.19	**0.75**	**0.63**	**0.85**	**0.77**	**0.83**	**−0.76**	**−0.73**

Bold values indicate significance (α = 0.05). WD, water depth; Al, aluminium; Fe, iron; S, sulphur; TOC, total organic carbon; $\delta^{13}C$, carbon isotopic composition; N, total nitrogen; $\delta^{15}N$, nitrogen isotopic composition; TIC, total inorganic carbon; OEP, odd-over-even predominance.

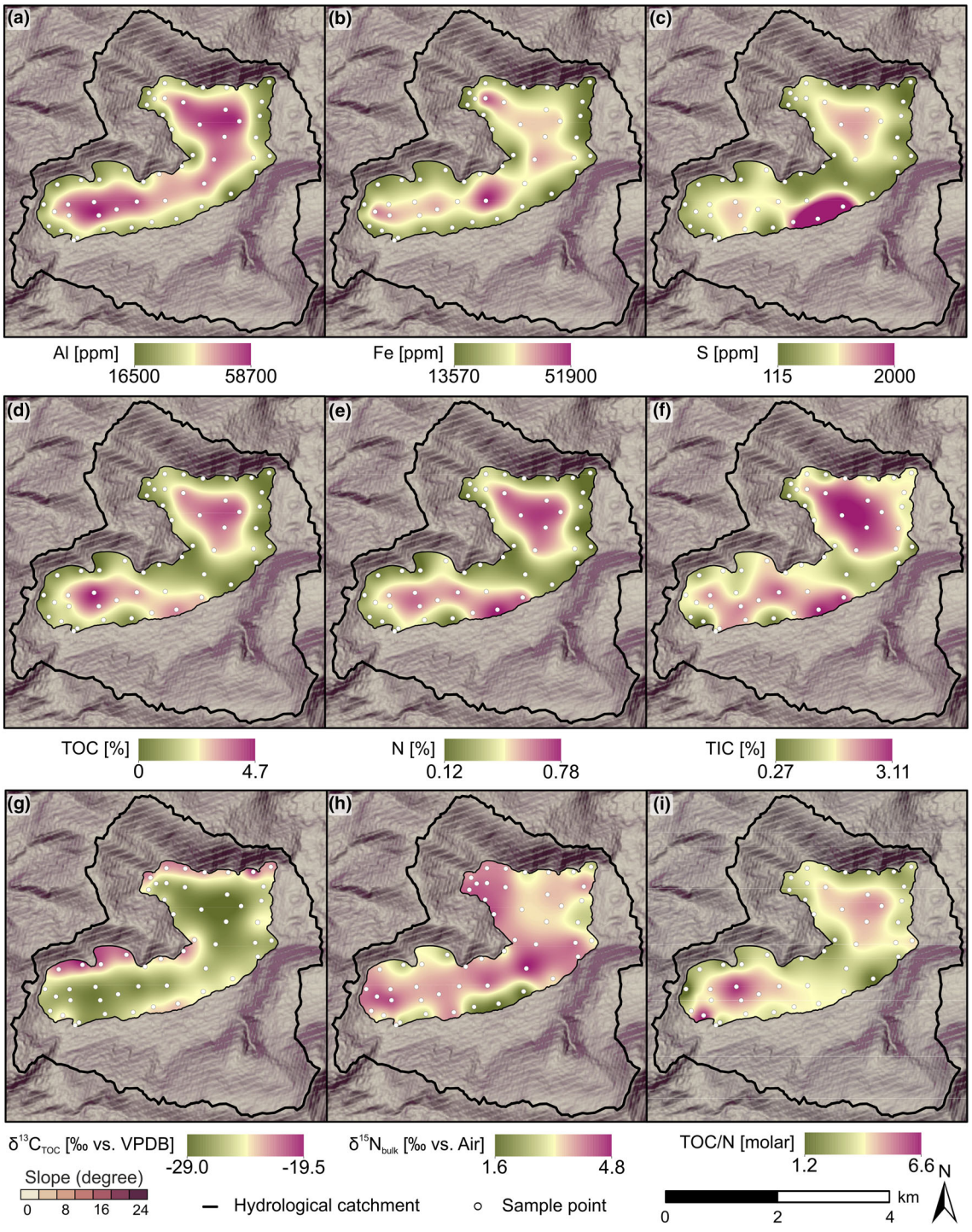

FIGURE 4 Spatial distribution of (a Al, (b) Fe, (c) S, (d) TOC, (e) N, (f) TIC, (g) $\delta^{13}C_{TOC}$, (h) $\delta^{15}N$ and (i) molar TOC/N ratio of Lake Khar Nuur. The lower and upper scale limit is based on the lowest and highest measured values. Note that for the distribution map of S an upper limit of 2,000 ppm instead of the detected 4,900 ± 500 ppm was used to highlight differences of the spatial distribution. Also shown are the slope and the catchment of Lake Khar Nuur

The spatial distribution of Al, Fe and TOC/N is also reflected in significant correlations with water depth (r: Al = 0.87, Fe = 0.81 and TOC/N = 0.59; $\alpha < 0.05$; Table 1). Although TOC, N and TIC are also significantly correlated with water depth (r between 0.56 and 0.75; $\alpha < 0.05$; Table 1) and Al (r between 0.61 and 0.80; $\alpha < 0.05$; Table 1), they correlate significantly with S and with each other (r values between 0.63 and 0.96; $\alpha < 0.05$; Table 1). The $\delta^{13}C_{TOC}$ and water depth significantly anti-correlate ($r = -0.72$; $\alpha < 0.05$; Table 1) indicating ^{13}C depleted $\delta^{13}C$ values at greater water depth and vice versa.

4.3 | *n*-Alkanes

The *n*-alkanes from plant and topsoil samples from sites with grasses/herbs and *Betula nana* (L.) in the Khar Nuur catchment show distinct differences in their chain-length distribution pattern (Figure 5). Sites with grasses/herbs show a nC_{31} dominance for both the plants and the respective topsoils (Figure 5a). The *n*-alkane concentration of the grass samples ranges from 440 to 3,260 μg g^{-1} and is distinctly lower for the topsoils (17 ± 14 μg g^{-1}). The grass samples show higher OEP values (24.5 ± 7.7) compared to the respective topsoil samples (8.4 ± 1.8). In contrast, sites covered with the shrub *Betula nana* (L.) show a distinct nC_{27} dominance (Figure 5b). The *n*-alkane concentration of the two *Betula nana* (L.) samples is 500 ± 20 μg g^{-1}, and 19 μg g^{-1} for the topsoil sample. Higher OEP values are shown by the *Betula nana* (L.) samples (27.0 ± 1.2) compared to the respective topsoil sample (14.5).

Based on our findings, we identified nC_{31} and nC_{27} as two end-members for the vegetation forms of grasses/herbs and shrubs in the Khar Nuur catchment, respectively, and calculated a modified *n*-alkane ratio to distinguish between both vegetation forms (cf. section 3.6). The *n*-alkane ratio of the sites with grasses/herbs is 0.91 ± 0.07 (plants) and 0.74 ± 0.08 (tospoils), and 0.12 ± 0.03 (plants) and 0.27 (topsoil) for sites with *Betula nana* (L.).

In the lake, the *n*-alkane concentration is the highest in both basins with values up to 12.7 μg g^{-1} in basin A and values up to 11.5 μg g^{-1} in basin B (Figure 6a). All other samples show concentrations < 9.7 μg g^{-1} with the lowest concentrations in the nearshore samples (Figure 6a). Both *n*-alkanes nC_{21} and nC_{31} show highest concentrations in the centre of basins A and B and follow the same pattern as the total *n*-alkane concentration (Figure 6b, c). It is notable that the concentration of nC_{21} (0.01–1.2 μg g^{-1}) is distinctly lower compared to nC_{31} (0.11–2.4 μg g^{-1}) (Figure 5b, c). The P_{aq}' ranges between 0.13 and 0.42 and shows highest values in the two basins with values between 0.36 and 0.42. All other samples show values < 0.32 (Figure 6e). The OEP ranges between 5.2 and 8.0 and shows low values for the samples located in the two basins (Figure 6d). High values are present in some samples located at the south-eastern, north-eastern and north-western shore (Figure 6d). The modified *n*-alkane ratio with regional end-members ranges between 0.53 and 0.71. The lowest values occur at the central southern shore and in both basins A and B (< 0.62), whereas highest values (0.65–0.71) are present in samples located at the shorelines of the lake. Exceptional with lower values is one shoreline sample west of the sub-aquatic ridge (Figure 6f).

Significant correlations exist between the spatial distribution of the *n*-alkane concentration, the *n*-alkanes nC_{21}, nC_{31} and the P_{aq}' (r between 0.67 and 0.99; $\alpha < 0.05$; Table 1). While the OEP is significantly anti-correlated with water depth ($r = -0.62$; $\alpha < 0.05$), there exists no significant correlation between the modified *n*-alkane ratio and water depth ($r = -0.23$; $\alpha > 0.05$; Table 1). Moreover, there is a significant anti-correlation between the P_{aq}' and the modified *n*-alkane ratio ($r = -0.73$; $\alpha < 0.05$; Table 1).

5 | DISCUSSION

5.1 | Allochthonous versus autochthonous sediment and inorganic and organic sediment compound origin in Khar Nuur sediments

Lake sediments and their inorganic and organic sediment compounds are a mixture of allochthonous material from the catchment and autochthonous material produced within the lake (Meyers & Ishiwatari, 1993). Therefore, it is an important precondition to disentangle both signals to robustly interpret transport processes, inorganic and organic sediment compound origin/sources and the environmental conditions under which they accumulate.

5.1.1 | Grain size and elements

A fundamental proxy to differentiate sediment transport energy and transport regimes in lake sediments is the grain size distribution. The most prominent sediment transport regimes can be identified by the Mode 1 which describes the most frequently occurring particle size in each sample (Blott & Pye, 2001). The grain size distribution in the

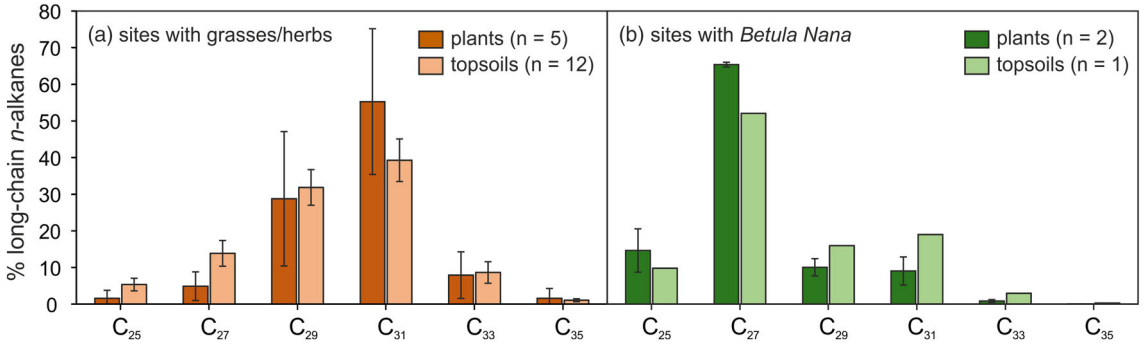

FIGURE 5 Chain length distribution patterns for long-chain *n*-alkanes in modern plants and topsoils from sites with (a) grasses/herbs and (b) the shrub *Betula nana* (L.) from the Khar Nuur catchment. For sample locations see Figure 1(d)

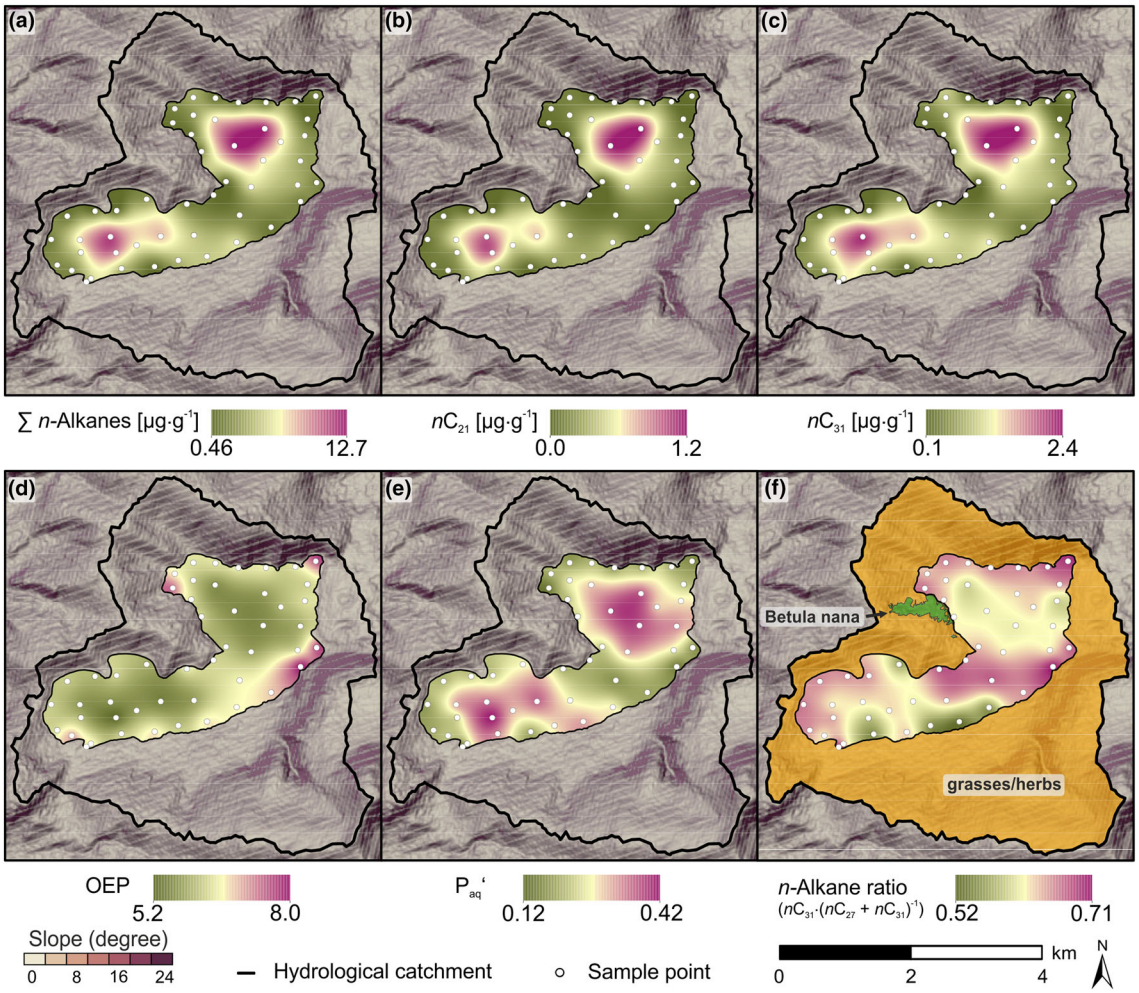

FIGURE 6 Spatial distribution of the (a) total *n*-alkane concentration, (b) concentration of nC_{21}, (c) concentration of nC_{31}, (d) odd-over-even predominance (OEP), (e) P_{aq}' and (f) *n*-alkane ratio ($nC_{31} \cdot (nC_{27} + nC_{31})^{-1}$). The lower and upper scale limit is based on the lowest and highest measured values. Also shown are the slope and the catchment of Lake Khar Nuur

surface sediments of Lake Khar Nuur exhibits high Mode 1 values in the nearshore samples compared to low values in the two basins (Figure 3b). Consequently, the grain size distribution follows the direction of sediment transport into the lake, indicating a higher energy regime near the shore and a lower energy regime towards the central part of the lake where sediments are focussed (Håkanson & Jansson, 1983; Mclaren & Bowles, 1985; Wang et al., 2015). This sediment focussing is likely caused by higher transport energies near the several small periodically inflows which mainly occur along the depth contours of the catchment during precipitation events and snow melt (Figure 1b). The clay and silt fractions are transported towards the lake centre of basins A and B where they can settle at calmer water conditions. Sediment focussing of the finer fractions in deeper waters of Lake Khar Nuur is further supported by the significant anti-correlation of water depth and Mode 1 ($r = -0.45$, $\alpha < 0.05$; Table 1; Figure 3b). This typical sediment distribution was also found in previous studies (Anderson et al., 2008; Thomas et al., 1972; Wang et al., 2015). It has to be noted that the > 2 mm fraction was removed before grain size measurements due to technical reasons. While the > 2 mm fraction was not quantified but present in some samples (grey sample points in Figure 3b), it is likely that the > 2 mm fraction would lead to higher Mode 1 values in those samples. However, the > 2 mm fraction was exclusively found in the nearshore samples which supports our findings that high transport energy regimes occur near the periodical inflows at the shoreline.

The decrease in grain size from the shoreline to the basins is accompanied by an increase in the concentration of the allochthonous elements Al and Fe. Both elements are typically bound to the fine grain size fraction (i.e. clay and feldspars) (e.g. Wen et al., 2008; Wündsch et al., 2018) and therefore significantly anti-correlate with the Mode 1 in Lake Khar Nuur ($r = -0.49$ and -0.55, respectively; $\alpha < 0.05$; Table 1; Figures 3b, 4a, b). Since Al and Fe are thought to be of allochthonous origin in lacustrine systems (Wen et al., 2008; Wündsch et al., 2018), their significant correlation with water depth ($r = 0.87$ and 0.81, respectively; $\alpha < 0.05$; Table 1) indicates the high accumulation of allochthonous material within the deep zones of basins A and B. According to Anderson et al. (2008, and references cited therein), sediment accumulation mostly occurs below a mud

deposition boundary depth which is further described by Wang et al. (2015) as the sediment accumulation zone that is least influenced by wind-driven turbulences and other processes. Thus, this accumulation zone provides the best suited sediments for paleoenvironmental studies, and for Lake Khar Nuur, a distinct sediment focussing occurs in the accumulation zones in the two basins A and B (Anderson et al., 2008; Lehman, 1975; Wang et al., 2015).

5.1.2 | Carbon and nitrogen contents and bulk isotopic composition

The accumulation zones in the two basins in Lake Khar Nuur are also evident in the characteristic spatial distribution of inorganic and organic sediment compounds. The highest TOC and N concentrations, as well as highest molar TOC/N ratios occur in both basins, resulting in significant correlations of TOC, N and TOC/N ratio with water depth (r = 0.75, 0.71 and 0.59, respectively; α < 0.05; Table 1; Figure 4d, e, i). Low molar TOC/N ratios in the two basins would classically indicate a predominantly autochthonous origin of organic material since values < 10 are thought to be representative for aquatic plants (Meyers, 1994). However, TOC, N and their molar ratio also significantly correlate with the allochthonous elements Al and Fe (Table 1) and indicate that organic matter cannot be exclusively of autochthonous origin in the accumulation zones. Those discrepancies could be possibly explained by (i) the heterogenic nature of organic matter that often comprises a mixed signal from allochthonous and autochthonous sources in lake sediments and (ii) the very low TOC and N concentrations of the nearshore samples that might bias the respective molar TOC/N ratios (Woszczyk et al., 2011). However, it is notable that hotspots with high TOC and N values are not only evident in the two basins, but also occur in the central southern part of the lake. Here, the site-related subcatchment is less steep and the well-developed soils favour the settlement of nomadic families and livestock grazing during summer. Thus, this observed hotspot of organic matter in the lake likely indicates increased input by erosion, mainly due to anthropogenic activity (cf. section 5.3).

Additional information about organic matter origin and environmental conditions under which the sediments become deposited might be provided by $\delta^{13}C_{TOC}$ and $\delta^{15}N$, although different fractionation factors can complicate the clear interpretation and source assignment of both isotopes (Meyers, 2003). The $\delta^{13}C_{TOC}$ values from Lake Khar Nuur are depleted in ^{13}C (−28.7 to −24.2‰) for most parts of the lake, except for the northern and central southern shorelines where $\delta^{13}C_{TOC}$ values are more enriched in ^{13}C (−23.9 to −19.6‰). Differences in $\delta^{13}C_{TOC}$ are often explained by the different photosynthetic pathway of C3 and C4 plants, but in the Khar Nuur catchment only plants using the C3 photosynthetic mode (Calvin–Benson pathway) grow, typically showing $\delta^{13}C$ values from −33 to −22‰ (Meyers, 1994; Pyankov et al., 2000). Changes in $\delta^{13}C$ of C3 plants indicate variations in plant water use efficiency and thus drought stress (Rao et al., 2017; Struck et al., 2020), but those changes in water use efficiency would only explain a few ‰ differences and not the large differences at the northern and central southern shoreline. Another explanation are aquatic plants that can have $\delta^{13}C_{TOC}$ values in the isotopic range of C3 plants (−30 to −25‰) when they use dissolved carbon dioxide (CO_2) from the water column which is in isotopic equilibrium with the atmosphere (Meyers, 1994). However, when the availability of dissolved atmospheric CO_2 ($\delta^{13}C$ = −7‰) is limited and aquatic plants begin to use dissolved bicarbonate ion (HCO_3^-) ($\delta^{13}C$ = 1‰), their isotopic composition becomes enriched in ^{13}C, resulting in up to 10‰ more positive $\delta^{13}C_{TOC}$ values (Bradley, 2015; Yu et al., 2015). The HCO_3^- origin in the lake from formerly deposited back-dissolved TIC can be of autochthonous origin by evaporitic carbonate precipitation and/or biogenic incorporation (formation of carbonate shells by plants and animals) (Jones & Bowser, 1978; Ju et al., 2010; Kelts & Hsü, 1978; Yu et al., 2018). Additionally, TIC can derive from allochthonous sources such as limestones in the catchment and/or aeolian dust which is an important carbon source in semi-arid regions (Jones & Bowser, 1978; Grunert & Lehmkuhl, 2004; Kelts & Hsü, 1978). Although we cannot completely rule out the contribution of allochthonous carbonates in the Khar Nuur sediments, they are rather unlikely because the bedrock of the catchment is not made of calcareous bedrock which is supported by modern ^{14}C-ages of a dated water plant and a surface sediment (see Supporting Information, Table S1). Thus, since the so-called 'hardwater effect' from old calcareous bedrock is not evident in the Khar Nuur catchment, TIC should mainly be derived from carbonate precipitation and biogenic sources. However, samples with ^{13}C enriched $\delta^{13}C_{TOC}$ values along the northern shore have likewise low TIC concentration. Therefore, we suggest that the strong enrichment is due to a dissolution of the formerly deposited inorganic carbon in the lake water and that the southward exposure of the northern shore enables enhanced aquatic productivity in the lake, also below the ice cover (eight to nine months) (Gibson et al., 1999; Loose et al., 2009). However, we have to mention that a more detailed picture of the TIC sources would be derived by further mineralogical analyses.

The $\delta^{15}N$ signal can also be used to investigate organic matter sources and biogeochemical processes in lake sediments (Meyers, 2003; Talbot, 2001; Zech et al., 2011). Aquatic plants often have more positive values (+8.5‰) compared to terrestrial plants (+0.5‰), because dissolved inorganic nitrogen is 7–10‰ more positive than atmosphere-derived nitrogen (Peterson & Howarth, 1987; Peters et al., 1978; Meyers, 2003). The $\delta^{15}N$ values in Lake Khar Nuur are mostly between 3 and 5‰, indicating a mixture of autochthonous and allochthonous organic matter. Distinctly low values only occur near the central southern shore and to some lesser degree close to the other shores, indicating a larger proportion of allochthonous organic matter in those samples. This is in line with the observed anthropogenic usage of this part of the catchment and the gully erosion (Figure 2c). While the $\delta^{13}C_{TOC}$ signal is not able to differentiate between the allochthonous input of C3 plants and autochthonous production from aquatic algae, the $\delta^{15}N$ signal identifies this hotspot of increased allochthonous input at the central southern shoreline.

5.1.3 | Leaf wax *n*-alkanes

A more homogenic part of the organic matter pool in lake sediments are *n*-alkanes. Based on their chain-length distribution one can differentiate whether they have a allochthonous origin from the leaf waxes of terrestrial plants (nC_{27}–nC_{35}) or a autochthonous origin from aquatic (submerged) macrophytes (nC_{21} and nC_{23}) (Bliedtner et al., 2018; Eglinton & Eglinton, 2008; Ficken et al., 2000; Sachse et al., 2004; Struck et al., 2020). In Lake Khar Nuur, the spatial distribution of the most abundant autochthonous (aquatic; nC_{21}) and allochthonous (terrestrial; nC_{31}) *n*-alkanes show highest concentrations in the accumulation zones in the deep basins and thus, underline the sedimentary focussing in the basins (Figure 6b, c). Compared with each other, allochthonous-derived nC_{31} show distinctly higher concentration in those accumulation zones than the autochthonous-derived nC_{21}. Consequently, the P_{aq}' shows lower values of 0.12 to 0.42 over the whole lake, indicating a variable mixture of allochthonous and autochthonous *n*-alkanes (Figure 6e). Although allochthonous *n*-alkanes dominate throughout the lake, notable autochthonous *n*-alkane contributions are present in the two basins of the lake (Figure 6e). Relatively high P_{aq}' values close to the central southern shore can be explained by enhanced autochthonous productivity due to anthropogenic activity and input of nutrients (see section 4.3). Overall, the *n*-alkane preservation is good with OEP values above 5, and higher values at some sites close to the shore probably document input of poorly degraded allochthonous *n*-alkanes.

It is important to note that *n*-alkanes represent only a small fraction of the total organic matter pool in lake sediments and are possibly less influenced by degradation effects on shorter timescale compared to TOC, N and their stable isotopes (Eglinton & Eglinton, 2008; Meyers, 2003). Nevertheless, this does not hamper the overall picture that the heterogenic organic matter pool as well as the more homogenic *n*-alkanes comprise a mixture of autochthonous and allochthonous organic matter sources.

5.2 | The vegetation distribution in Khar Nuur sediments using leaf wax *n*-alkanes

Long-chain *n*-alkanes have the potential to differentiate between vegetation types by their homologue patterns (Bliedtner et al., 2018; Marseille et al., 1999; Schwark et al., 2002). The fundamental assumption of this approach is that the *n*-alkane chain-lengths C_{27} and C_{29} are thought to be produced by deciduous trees/shrubs and the chain-lengths C_{31} and C_{33} by grasses/herbs (Bliedtner et al., 2018; Marseille et al., 1999; Schwark et al., 2002). This holds also true for the Khar Nuur catchment, where distinct differences in the leaf wax patterns are apparent for sites dominated by grasses/herbs and sites dominated by the shrub *Betula nana* (L.) (Figure 2b). Plant samples and their respective topsoils show that sites with grasses/herbs are dominated by nC_{31}, whereby sites with the shrubby *Betula nana* (L.) are dominated by nC_{27} (Figure 5). Those findings are underlined by recent calibration studies from Mongolia and China, where grasses/herbs show a nC_{31} predominance and *Betula platyphylla* show a nC_{27} predominance (Wang et al., 2018; Struck et al., 2020). Thus, leaf wax *n*-alkane patterns have the potential to differentiate between both vegetation types in the Khar Nuur catchment and contributions from the respective vegetation types should be differentiated in the Khar Nuur sediment surface samples (see section 4.3; Figure 5). To disentangle both vegetation types, we applied a modified normalized *n*-alkane ratio (cf. section 2.3.4; Equation 3; Figure 6f). However, the distinct differences of the *n*-alkane ratio for grasses/herbs (values > 0.66) and *Betula nana* (L.) (values < 0.27) found in modern plants and topsoils are not reflected in the lake surface samples (0.52–0.71) that show rather a grass/herb signal for the whole lake than a *Betula nana* (L.) signal. These findings are partly unexpected for the nearshore samples KN28 and KN35 in basin A (see Figure 1b, c), because *Betula nana* (L.) is present in the respective sub-catchments of those samples and could possibly yield lower values of the *n*-alkane ratio. Instead, those nearshore surface sediment samples reflect a grass signal rather than a *Betula nana* (L.) signal. Because both vegetation types produce similar amounts of *n*-alkanes in the Khar Nuur catchment (except one grass sample from the southern part of the catchment, see Table S2), we suggest that *n*-alkanes from the grass sites and the grassy undergrowth of the *Betula nana* (L.) sites in this sub-catchment are apparent in greater amounts and contribute to the grass dominated *n*-alkane ratio in those nearshore samples. The other surface sediment samples reflect the grass/herb signal of their respective sub-catchments, however, lower values from the *n*-alkane ratio are present at the central southern shore (0.52–0.55). Here, the aforementioned allochthonous input of eroded topsoil material possibly leads to higher production rates of aquatic (algae) *n*-alkanes via nutrient loading, which can also produce to some amounts the chain-length nC_{27} (Ficken et al., 2000) and possibly contribute to the *n*-alkane ratio. In this context, it is notable that the P_{aq}' and the *n*-alkane ratio are significantly anti-correlated ($r = -0.73$; $\alpha < 0.05$; Table 1) in the Khar Nuur sediments, indicating possible contributions from aquatic plants also on the longer chain nC_{27}. Thus, possible aquatic biases to the longer chains would complicate a clear interpretation of the *n*-alkane ratio in terms of vegetation types, although the grass/herb-derived proportion of nC_{31} dominates in all samples. Overall, the *n*-alkane ratio enables differentiation between the vegetation types of modern plants and respective topsoils in the Khar Nuur catchment, i.e. between grasses/herbs and *Betula nana* (L.). However, those differences are not reflected in the sediment samples from Lake Khar Nuur and vegetation reconstructions might be biased by aquatic *n*-alkane contributions.

5.3 | Traces of anthropogenic activity reflected in Khar Nuur sediments

In semi-arid Mongolia, anthropogenic activity has strongly influenced soil erosion and landscape changes since the introduction of horse-borne mobile pastoralism ~5 cal. ka BP (Fernández-Giménez et al., 2017; Taylor et al., 2020). Even today, large parts of the country are

used by nomadic pastoralism with large herds of sheep, goats, camels, cows/yaks and horses (Upton, 2010). However, (over-)grazing in semi-arid regions strongly influences landscape stability since physical soil compaction (trampling) and removal of vegetation cover favours both sheet and gully erosion and thus the irreversible loss of fine particles by erosion (Wiesmeier et al., 2015).

The Khar Nuur catchment is settled by many nomadic families and their large herds during summertime. Although the northern steep slopes of the catchment are only covered by very shallow soils and marginal vegetation, animals graze there. In contrast, especially the flatter areas in the southern part of the Khar Nuur catchment are ideal sites where the majority of grazing and family housing takes place (Figures 1d, 2a). As a result of grazing and soil exposure to weathering and erosion, several gullies in the southern part of the catchment developed deeply in the well-developed soils (Figure 2c). This anthropogenic-induced soil erosion can be traced in the surface samples of Lake Khar Nuur.

High TOC and N values are accompanied by slightly ^{13}C enriched $\delta^{13}C_{TOC}$ values and distinctly ^{15}N depleted $\delta^{15}N$ values at the central southern shore, indicating that large proportions of allochthonous-derived organic matter became preferentially eroded from the southern part of the catchment. Although it has to be noted that TOC and N and their isotopic composition are not direct evidence for anthropogenic activity, both show values that are high for sites outside the accumulation zones. Strongly ^{15}N depleted $\delta^{15}N$ values at the southern shore are likewise exceptional compared to the other parts of the lake and might indicate the input of organic matter from allochthonous sources. Consequently, the most likely cause for the observed TOC, N and $\delta^{15}N$ distribution at the southern shore is soil erosion induced by the extensive nearby anthropogenic activity.

Those findings are supported by the conspicuous distribution of the element S, which shows highest concentrations at the central southern shore (Figure 4c). Sulphur is a part of the proteinogenic amino acids which are involved in several enzyme-reactions during the degradation of plants and faunal remains in the digestive tract and partly defecated (Brosnan & Brosnan, 2006; Kertesz & Mirleau, 2004). Consequently, S from faunal and human faeces in the central southern part of the Khar Nuur catchment can be stored in the catchment soils and eroded into the lake and/or directly transported into the lake with the faeces by surficial flow. Thus, high S concentrations at the central southern shore could be a further indicator of high allochthonous input through anthropogenic activity and soil erosion.

Traces of anthropogenic activity and soil erosion in the Khar Nuur sediments are further supported by the significant correlation of TOC, N and S (r between 0.66 and 0.96; $\alpha < 0.05$). Thus, anthropogenic activity in the catchment by grazing and human occupation most likely leads to the characteristic spatial distribution of those elements in the lake. However, trace-elements of anthropogenic activity are difficult to disentangle and more detailed analyses of source-specific biomarkers are necessary to confirm this assumption.

6 | CONCLUSIONS

Our grain size and biogeochemical investigations on surface sediment samples from Lake Khar Nuur, a small lake with a small hydrological catchment from the Mongolian Altai, gave the following results:

- The grain size distribution shows higher transport energy levels at the shoreline compared to the two basins of Lake Khar Nuur. The accumulation of finer sediments in those basins is accompanied by high amounts of the inorganic sediment compounds Al and Fe, which are of allochthonous origin. Consequently, the two basins act as the main sediment accumulation zones where sediment focussing is observed.
- Disentangling the autochthonous and allochthonous origin of organic material in the surface sediments is not trivial. While TOC and N accumulate preferentially in the accumulation zones, molar TOC/N ratios indicate high autochthonous production throughout the lake, which is mostly underlined by ^{15}N enriched $\delta^{15}N$ values. The respective ^{13}C depleted $\delta^{13}C_{TOC}$ values could indicate contributions from both allochthonous C3 plants and autochthonous production or at the shorelines changes in available dissolved inorganic carbon (CO_2) for aquatic use. However, those proxies reflect the whole heterogeneous organic matter pool which most likely comprise a mixture of both allochthonous and autochthonous sources. In contrast, the more homogenous and source-specific *n*-alkanes are constituents of the organic matter pool and indicate that *n*-alkanes from allochthonous and autochthonous sources are apparent in the surface sediments with higher proportion of allochthonous compounds compared to autochthonous ones.
- Leaf wax-derived long-chain *n*-alkanes in modern plants and topsoils enables differentiation between the dominating vegetation types in the Khar Nuur catchment, i.e. between grasses/herbs and the shrub *Betula nana* (L.). Grasses/herbs show a distinct nC_{31} predominance and *Betula nana* (L.) a dominance of nC_{27}. However, those differences are not reflected in the surface sediment samples from Lake Khar Nuur, where nC_{31} is the dominant *n*-alkane throughout the lake. This indicates that grasses become preferentially incorporated into the lake, also at those sites in the catchment where *Betula nana* (L.) is growing.
- Anthropogenic activity in the southern Khar Nuur catchment is clearly observable in the surface sediments from the central southern shoreline since TOC, N and $\delta^{15}N$ indicate increased allochthonous input that is most likely due to increased soil erosion. This is accompanied by increased input of faecal remains as possibly indicated by increased contributions from the element S. However, those are only indirect indicators of anthropogenic activity and more direct analyses such as source-specific biomarkers are necessary to confirm this assumption.

Overall, sediments deposited in the accumulation zones in the two basins of Lake Khar Nuur reflect the recent environmental conditions of the lake and its hydrological catchment and are therefore ideal sediments for paleoenvironmental reconstructions. However, the proxies

which possibly will be used in such paleoenvironmental studies have to be carefully evaluated by modern reference studies, although one has to be aware that environmental changes can affect the spatial distribution of sediment compounds through time. Future work on surface sediments should focus on dating the different organic matter compounds for more information about the time of the integrated signal, as well as on compound-specific isotopes of the more homogenous organic matter compounds.

DECLARATION OF COMPETING INTEREST

The authors declare no competing interests.

DATA AVAILABILITY STATEMENT

All data used in this study is available either from the corresponding author on reasonable request or from the public resources as referenced in the text.

ACKNOWLEDGEMENTS

The authors would like to thank the Ernst Abbe Stiftung for financial support of the field trip to Mongolia in 2019. PS gratefully acknowledges the support by a fellowship from the state of Thuringia (Landesgraduiertenstipendium). The authors want to thank their logistic partners in Mongolia and all field trip participants in 2018 and 2019 for their helping hands in the field. Particularly acknowledged are M. Mulan, M. Muder, H.J. Schulze, G. Daut and T. Kasper for discussion and laboratory work. Special thanks go to N. Blaubach for assistance in the laboratory and to J. Labrie for providing the modified version of Gradistat 4.5. The authors thank two anonymous reviewers for their valuable and helpful comments on this article.

ORCID

P. Strobel https://orcid.org/0000-0002-7860-5398
J. Struck https://orcid.org/0000-0001-6102-7547
M. Bliedtner https://orcid.org/0000-0002-4109-9014

REFERENCES

Anderson, N.J. (1990) Spatial pattern of recent sediment and diatom accumulation in a small, monomictic, eutrophic lake. *Journal of Paleolimnology*, 3, 143–160.

Anderson, M.A., Whiteaker, L., Wakefield, E. & Amrhein, C. (2008) Properties and distribution of sediment in the Salton Sea, California: An assessment of predictive models. *Hydrobiologia*, 604, 97–110.

Bliedtner, M., Schäfer, I.K., Zech, R. & von Suchodoletz, H. (2018) Leaf wax n-alkanes in modern plants and topsoils from eastern Georgia (Caucasus) – Implications for reconstructing regional paleovegetation. *Biogeosciences*, 15, 3927–3936.

Blott, S.J. & Pye, K. (2001) GRADISTAT: A grain size distribution and statistics package for the analysis of unconsolidated sediments. *Earth Surface Processes and Landforms*, 26, 1237–1248.

Bradley, R.S. (2015) Chapter 9 - Lake Sediments. In: Bradley, R.S. (Ed.) *Paleoclimatology*, Third edn. San Diego, CA: Academic Press, pp. 319–343.

Brosnan, J.T. & Brosnan, M.E. (2006) The sulfur-containing amino acids: An overview. *The Journal of Nutrition*, 136, 1636S–1640S.

Buggle, B., Wiesenberg, G.L.B. & Glaser, B. (2010) Is there a possibility to correct fossil n-alkane data for postsedimentary alteration effects? *Applied Geochemistry*, 25, 947–957.

Bush, R.T. & McInerney, F.A. (2013) Leaf wax *n*-alkane distributions in and across modern plants: Implications for paleoecology and chemotaxonomy. *Geochimica et Cosmochimica Acta*, 117, 161–179.

Dearing, J.A. (1997) Sedimentary indicators of lake-level changes in the humid temperate zone: A critical review. *Journal of Paleolimnology*, 18, 1–14.

DeBusk, G.H. (1997) The distribution of pollen in the surface sediments of Lake Malaw^i, Africa, and the transport of pollen in large lakes. *Review of Palaeobotany and Palynology*, 97, 123–153.

DWD Climate Data Center. (2020) Recent and historical dataset: Monthly means of precipitation totals, montly mean air temperature and highest daily maximum temperature of a month for station Tolbo Sum (CDC-ID 44217) worldwide, version recent, last accessed: 2020-02-08. https://opendata.dwd.de/climate_environment/CDC/observations_global/CLIMAT/

Eglinton, T.I. & Eglinton, G. (2008) Molecular proxies for paleoclimatology. *Earth and Planetary Science Letters*, 275, 1–16.

Fernández-Giménez, M.E., Venable, N.H., Angerer, J., Fassnacht, S.R., Reid, R.S. & Khishigbayar, J. (2017) Exploring linked ecological and cultural tipping points in Mongolia. *Anthropocene*, 17, 46–69.

Ficken, K.J., Li, B., Swain, D.L. & Eglinton, G. (2000) An n-alkane proxy for the sedimentary input of submerged/floating freshwater aquatic macrophytes. *Organic Geochemistry*, 31, 745–749.

Gibson, J.A.E., Trull, T., Nichols, P.D., Summons, R.E. & McMinn, A. (1999) Sedimentation of 13C-rich organic matter from Antarctic sea-ice algae: A potential indicator of past sea-ice extent. *Geology*, 27, 331–334.

Grunert, J. & Lehmkuhl, F. (2004) Aeolian sedimentation in arid and semi-arid environments of western Mongolia. In: Smykatz-Kloss, W. & Felix-Henningsen, P. (Eds.) *Paleoecology of Quaternary Drylands*. Berlin: Springer, pp. 195–218.

Guo, B., Liu, Y., Zhang, F., Hou, J., Zhang, H. & Li, C. (2018) Heavy metals in the surface sediments of lakes on the Tibetan Plateau, China. *Environmental Science and Pollution Research*, 25, 3695–3707.

Håkanson, L. & Jansson, M. (1983) Principles of lake sedimentology. Springer; Berlin.

Hoefs, M.J.L., Rijpstra, W.I.C. & Sinninghe Damsté, J.S. (2002) The influence of oxic degradation on the sedimentary biomarker record I: Evidence from Madeira Abyssal Plain turbidites. *Geochimica et Cosmochimica Acta*, 66, 2719–2735.

Jones, B.F. & Bowser, C.J. (1978) The Mineralogy and Related Chemistry of Lake Sediments. In: Lerman, A. (ed.) *Lakes: Chemistry, Geology, Physics*. New York, NY: Springer. 179–235.

Ju, J., Zhu, L.-P., Wang, J., Xie, M., Zhen, X., Wang, Y. *et al.* (2010) Water and sediment chemistry of Lake Pumayum Co, South Tibet, China: Implications for interpreting sediment carbonate. *Journal of Paleolimnology*, 43, 463–474.

Kastner, S., Ohlendorf, C., Haberzettl, T., Lücke, A., Mayr, C., Maidana, N.I. *et al.* (2010) Southern hemispheric westerlies control the spatial distribution of modern sediments in Laguna Potrok Aike, Argentina. *Journal of Paleolimnology*, 44, 887–902.

Kelts, K. & Hsü, K.J. (1978) Freshwater Carbonate Sedimentation. In: Lerman, A (Ed.) *Lakes: Chemistry, Geology, Physics*. New York, NY: Springer, pp. 295–323.

Kertesz, M.A. & Mirleau, P. (2004) The role of soil microbes in plant sulphur nutrition. *Journal of Experimental Botany*, 55, 1939–1945.

Lehman, J.T. (1975) Reconstructing the rate of accumulation of lake sediment: The effect of sediment focusing. *Quaternary Research*, 5, 541–550.

Li, Q. (2018) Spatial variability and long-term change in pollen diversity in Nam co catchment (central Tibetan Plateau): Implications for alpine vegetation restoration from a paleoecological perspective. *Science China Earth Sciences*, 61, 270–284.

Li, Q. (2019) Distribution and vegetation representation of pollen assemblages from surface sediments of Nam Co, a large alpine lake in the

central Tibetan Plateau. *Vegetation History and Archaeobotany*, 28, 365–377.

Lie, U. & Pamatmat, M.M. (1965) Digging characteristics and sampling efficiency of the 0.1 m^2 Van Veen Grabb1. *Limnology and Oceanography*, 10, 379–384.

Liu, J., An, Z. & Liu, H. (2018) Leaf wax n-alkane distributions across plant types in the central Chinese Loess Plateau. *Organic Geochemistry*, 125, 260–269.

Loose, B., McGillis, W.R., Schlosser, P., Perovich, D. & Takahashi, T. (2009) Effects of freezing, growth, and ice cover on gas transport processes in laboratory seawater experiments. *Geophysical Research Letters*, 36.

Marseille, F., Disnar, J.R., Guillet, B. & Noack, Y. (1999) N-alkanes and free fatty acids in humus and A1 horizons of soils under beech, spruce and grass in the Massif-Central (Mont-Lozère), France. *European Journal of Soil Science*, 50, 433–441.

Martens, K. & Tudorancea, C. (1991) Seasonally and spatial distribution of the ostracods of Lake Zwai, Ethiopia (Crustacea: Ostracoda). *Freshwater Biology*, 25, 233–241.

Mclaren, P. & Bowles, D. (1985) The effects of sediment transport on grain-size distributions. *Journal of Sedimentary Petrology*, 55, 457–470.

Meyers, P.A. (1994) Preservation of elemental and isotopic source identification of sedimentary organic-matter. *Chemical Geology*, 114, 289–302.

Meyers, P.A. (2003) Applications of organic geochemistry to paleolimnological reconstructions: A summary of examples from the Laurentian Great Lakes. *Organic Geochemistry*, 34, 261–289.

Meyers, P.A. & Ishiwatari, R. (1993) Lacustrine organic geochemistry—An overview of indicators of organic matter sources and diagenesis in lake sediments. *Organic Geochemistry*, 20, 867–900.

Moore, J.W. (1980) Distribution and transport of heavy-metals in the sediments of a small northern eutrophic Lake. *Bulletin of Environmental Contamination and Toxicology*, 24, 828–833.

Oldfield, F. (1977) Lakes and their drainage basins as units of sediment-based ecological study. *Progress in Physical Geography: Earth and Environment*, 1, 460–504.

Onyari, J.M. & Wandiga, S.O. (1989) Distribution of Cr, Pb, Cd, Zn, Fe and Mn in Lake Victoria sediments, East-Africa. *Bulletin of Environmental Contamination and Toxicology*, 42, 807–813.

Peters, K.E., Sweeney, R.E. & Kaplan, I.R. (1978) Correlation of carbon and nitrogen stable isotope ratios in sedimentary organic matter 1. *Limnology and Oceanography*, 23, 598–604.

Planet Team. (2017) *Planet application program interface: In space for life on Earth*. San Francisco, CA: Planet Team.

Peterson, B.J. & Howarth, R.W. (1987) Sulfur, carbon, and nitrogen isotopes used to trace organic matter flow in the salt-marsh estuaries of Sapelo Island, Georgia1. *Limnology and Oceanography*, 32, 1195–1213.

Pyankov, V.I., Gunin, P.D., Tsoog, S. & Black, C.C. (2000) C4 plants in the vegetation of Mongolia: Their natural occurrence and geographical distribution in relation to climate. *Oecologia*, 123, 15–31.

Rao, Z., Guo, W., Cao, J., Shi, F., Jiang, H. & Li, C. (2017) Relationship between the stable carbon isotopic composition of modern plants and surface soils and climate: A global review. *Earth-Science Reviews*, 165, 110–119.

Sachse, D., Radke, J. & Gleixner, G. (2004) Hydrogen isotope ratios of recent lacustrine sedimentary n-alkanes record modern climate variability. *Geochimica et Cosmochimica Acta*, 68, 4877–4889.

Schäfer, I.K., Lanny, V., Franke, J., Eglinton, T.I., Zech, M., Vysloužilová, B. & Zech, R. (2016) Leaf waxes in litter and topsoils along a European transect. *The Soil*, 2, 551–564.

Schwark, L., Zink, K. & Lechterbeck, J. (2002) Reconstruction of postglacial to early Holocene vegetation history in terrestrial central Europe via cuticular lipid biomarkers and pollen records from lake sediments. *Geology*, 30, 463–466.

Shah, R.A., Achyuthan, H., Lone, A.M. & Ramanibai, R. (2017) Diatoms, spatial distribution and physicochemical characteristics of the Wular lake sediments, Kashmir valley, Jammu and Kashmir. *Journal of the Geological Society of India*, 90, 159–168.

Shepherd, T. & Wynne Griffiths, D. (2006) The effects of stress on plant cuticular waxes. *New Phytologist*, 171, 469–499.

Shuman, B. (2003) Controls on loss-on-ignition variation in cores from two shallow lakes in the northeastern United States. *Journal of Paleolimnology*, 30, 371–385.

Struck, J., Bliedtner, M., Strobel, P., Schumacher, J., Bazarradnaa, E. & Zech, R. (2020) Leaf wax n-alkane patterns and compound-specific δ13C of plants and topsoils from semi-arid and arid Mongolia. *Biogeosciences*, 17, 567–580.

Talbot, M.R. (2001) Nitrogen Isotopes in Palaeolimnology. In: Last, W.M., & Smol, J.P. (Eds.) *Tracking Environmental Change Using Lake Sediments: Physical and Geochemical Methods*. Dordrecht: Springer Netherlands, pp. 401–439.

Taylor, W., Fantoni, M., Marchina, C., Lepetz, S., Bayarsaikhan, J., Houle, J.-L. *et al.* (2020) Horse sacrifice and butchery in Bronze Age Mongolia. *Journal of Archaeological Science: Reports*, 31, 102313.

Thomas, R.L., Lewis, C.F.M. & Kemp, A.L.W. (1972) Distribution, composition and characteristics of surficial sediments of Lake Ontario. *Journal of Sedimentary Petrology*, 42, 66.

Upton, C. (2010) Living off the land: Nature and nomadism in Mongolia. *Geoforum*, 41, 865–874.

Vogel, H., Wessels, M., Albrecht, C., Stich, H.B. & Wagner, B. (2010) Spatial variability of recent sedimentation in Lake Ohrid (Albania/Macedonia). *Biogeosciences*, 7, 3333–3342.

Walther, M., Dashtseren, A., Kamp, U., Temujin, K., Meixner, F., Pan, C.G. *et al.* (2017) Glaciers, permafrost and Lake levels at the Tsengel Khairkhan Massif, Mongolian Altai, during the Late Pleistocene and Holocene. *Geosciences*, 7, 73.

Wang, J., Zhu, L., Wang, Y., Ju, J., Daut, G. & Li, M. (2015) Spatial variability and the controlling mechanisms of surface sediments from Nam Co, central Tibetan Plateau, China. *Sedimentary Geology*, 319, 69–77.

Wang, J., Axia, E., Xu, Y., Wang, G., Zhou, L., Jia, Y., Chen, Z. *et al.* (2018) Temperature effect on abundance and distribution of leaf wax n-alkanes across a temperature gradient along the 400 mm isohyet in China. *Organic Geochemistry*, 120, 31–41.

Wen, L.-S., Warnken, K.W. & Santschi, P.H. (2008) The role of organic carbon, iron, and aluminium oxyhydroxides as trace metal carriers: Comparison between the Trinity River and the Trinity River estuary (Galveston Bay, Texas). *Marine Chemistry*, 112, 20–37.

Wiesmeier, M., Munro, S., Barthold, F., Steffens, M., Schad, P. & Kögel-Knabner, I. (2015) Carbon storage capacity of semi-arid grassland soils and sequestration potentials in northern China. *Global Change Biology*, 21, 3836–3845.

Woszczyk, M., Bechtel, A., Gratzer, R., Kotarba, M.J., Kokociński, M., Fiebig, J. *et al.* (2011) Composition and origin of organic matter in surface sediments of Lake Sarbsko: A highly eutrophic and shallow coastal lake (northern Poland). *Organic Geochemistry*, 42, 1025–1038.

Wündsch, M., Haberzettl, T., Cawthra, H.C., Kirsten, K.L., Quick, L.J., Zabel, M. *et al.* (2018) Holocene environmental change along the southern Cape coast of South Africa – Insights from the Eilandvlei sediment record spanning the last 8.9 kyr. *Global and Planetary Change*, 163, 51–66.

Yu, Z.T., Wang, X.J., Zhang, E.L., Zhao, C.Y. & Liu, X.Q. (2015) Spatial distribution and sources of organic carbon in the surface sediment of Bosten Lake, China. *Biogeosciences*, 12, 6605–6615.

Yu, Z., Wang, X., Han, G., Liu, X. & Zhang, E. (2018) Organic and inorganic carbon and their stable isotopes in surface sediments of the Yellow River estuary. *Scientific Reports*, 8, 10825.

Yu, S., Wang, J., Li, Y., Peng, P., Kai, J., Kou, Q. *et al.* (2019) Spatial distribution of diatom assemblages in the surface sediments of Selin Co, central Tibetan Plateau, China, and the controlling factors. *Journal of Great Lakes Research*, 45, 1069–1079.

Zalat, A. & Vildary, S.S. (2005) Distribution of diatom assemblages and their relationship to environmental variables in the surface sediments of three northern Egyptian lakes. *Journal of Paleolimnology*, 34, 159–174.

Zech, M., Buggle, B., Leiber, K., Marković, S., Glaser, B., Hambach, U. *et al.* (2010) Reconstructing quaternary vegetation history in the Carpathian Basin, SE-Europe, using n-alkane biomarkers as molecular fossils: Problems and possible solutions, potential and limitations. *Quaternary International*, 58, 148–155.

Zech, M., Bimüller, C., Hemp, A., Samimi, C., Broesike, C., Hörold, C. *et al.* (2011) Human and climate impact on 15N natural abundance of plants and soils in high-mountain ecosystems: A short review and two examples from the eastern Pamirs and Mt. Kilimanjaro. *Isotopes in Environmental and Health Studies*, 47, 286–296.

Zhao, Y., Sayer, C.D., Birks, H.H., Hughes, M. & Peglar, S.M. (2006) Spatial representation of aquatic vegetation by macrofossils and pollen in a small and shallow Lake. *Journal of Paleolimnology*, 35, 335–350.

SUPPORTING INFORMATION

Additional supporting information may be found online in the Supporting Information section at the end of this article.

How to cite this article: Strobel P, Struck J, Zech R, Bliedtner M. The spatial distribution of sedimentary compounds and their environmental implications in surface sediments of Lake Khar Nuur (Mongolian Altai). *Earth Surf. Process. Landforms*. 2021;1–16. https://doi.org/10.1002/esp.5049